Published in final edited form as:
Int J Cancer. 2013 April 15; 132(8): 1860–1867. doi:10.1002/ijc.27872.

Targeted imaging of breast tumor progression and therapeutic response in a human uMUC-1 expressing transgenic mouse model

Subrata K. Ghosh[1], **Masashi Uchida**[1], **Byunghee Yoo**[1], **Alana W. Ross**[1], **Sandra J. Gendler**[2], **Jianlin Gong**[3], **Anna Moore**[1,*], and **Zdravka Medarova**[1,*]

[1]Molecular Imaging Laboratory, MGH/HST Athinoula A. Martinos Center for Biomedical Imaging, Department of Radiology, Massachusetts General Hospital/Harvard Medical School, Boston, MA

[2]Department of Biochemistry and Molecular Biology, Mayo Clinic, Scottsdale, AZ

[3]Department of Medicine, Boston University School of Medicine, 650 Albany Street, Boston, MA

Abstract

The ability to monitor breast cancer initiation and progression on the molecular level would provide an effective tool for early diagnosis and therapy. In the present study, we focused on the underglycosylated MUC-1 tumor antigen (uMUC-1), which is directly linked to tumor progression from pre-malignancy to advanced malignancy in breast cancer and has been identified as the independent predictor of local recurrence and tumor response to chemotherapy. We investigated whether changes in uMUC-1 expression during tumor development and therapeutic intervention could be monitored non-invasively using molecular imaging approach with the uMUC-1-specific contrast agent (MN-EPPT) detectable by magnetic resonance and fluorescence optical imaging. This was done in mice that express human uMUC-1 tumor antigen (MMT mice) and develop spontaneous mammary carcinoma in a stage-wise fashion. After the injection of MN-EPPT there was a significant reduction in average T2 relaxation times of the mammary fat pad between pre-malignancy and cancer. In addition, T2 relaxation times were already altered at pre-malignant state in these mice compared to non-tumor bearing mice. This indicated that targeting uMUC-1 could be useful for detecting pre-malignant transformation in the mammary fat pad. We also probed changes in uMUC-1 expression with MN-EPPT during therapy with doxorubicin. We observed that tumor delta-T2s were significantly reduced by treatment with doxorubicin indicating lower accumulation of MN-EPPT. This correlated with a lower level of MUC-1 expression in the doxorubicin-treated tumors, as confirmed by immunoblotting. Our study could provide a very sensitive molecular imaging approach for monitoring tumor progression and therapeutic response.

Introduction

It is becoming clear that cancer cells undergo specific molecular transformations long before there is a detectable tumor. The ability to diagnose cancer at these earliest stages of molecular dysregulation before any overt physiologic symptoms have developed, would

*Address correspondence to: Anna Moore, Ph.D., Zdravka Medarova, Ph.D., Molecular Imaging Laboratory, MGH/MIT/HMS Athinoula A. Martinos Center for Biomedical Imaging, Massachusetts General Hospital/ Harvard Medical School, Building 75, 13th Street, Charlestown, MA 02129. Tel. 617-724-0540, Fax 617-643-4865, amoore@helix.mgh.harvard.edu, zmedarova@partners.org.

This study focuses on the underglycosylated MUC-1 tumor antigen (uMUC-1), which is directly linked to breast cancer progression and tumor response to chemotherapy. We showed that changes in uMUC-1 expression during tumor development and therapeutic intervention could be monitored non-invasively using molecular imaging approach with the uMUC-1-specific contrast agent. Our study could provide a very sensitive molecular approach for monitoring tumor progression and therapeutic response as well as for identifying pre-malignancy in breast cancer.

permit much more adequate therapeutic intervention and would represent an additional step in the direction of transforming cancer into an overall curable disease. Towards this goal, the conception of molecularly targeted diagnostic approaches allows for identification of the precursor dysregulation that leads to cancer and for directing clinical intervention towards prevention rather than therapy.

Underglycosylated mucin-1 tumor antigen (uMUC-1) is overexpressed and underglycosylated in over 90% of human breast cancers including triple negative cancers[1–6] and has been identified as a promising biomarker candidate. During tumorigenesis it undergoes well-defined molecular changes manifested as an increase in expression, more extensive deglycosylation, and ubiquitous expressed all over the cell surface[7–11]. The value of uMUC-1 for tumor staging is especially high because it is expressed very early in the transformation process. In fact, uMUC-1 overexpression has been implicated as a causative factor for tumorigenesis in a breast cancer model[12]. In humans, aberrant expression of uMUC1 has been found in atypical ductal hyperplasia lesions, which indicates a higher risk for developing subsequent invasive breast carcinoma[13]. uMUC-1 was also found in ductal carcinoma in situ[13, 14] and, remarkably, among other markers was identified as the only independent predictor of local recurrence[14].

In addition to being an excellent marker for the prediction and characterization of tumor progression, uMUC-1 availability is also directly related to treatment outcome, making this target antigen one of the most widely used markers of therapeutic response and disease recurrence, particularly in patients with locally advanced and invasive disease[15]. After treatment with neoadjuvant chemotherapy, a consistent reduction in uMUC-1 levels was observed, suggesting that it can be explored as an intermediate biomarker for assessment of therapeutic response and prognosis[16]. Since uMUC-1 plays a critical role in cancer proliferation and metastasis, its downregulation following therapeutic intervention decreases the invasive potential of cancer cells, reduces metastatic burden, and improves survival[17–19].

Because of the high importance of the uMUC-1 antigen for cancer progression and therapy it would be highly advantageous to follow its expression longitudinally and non-invasively in breast cancer patients. With this goal in mind we developed a molecular imaging approach to track uMUC-1 expression over the entire course of the pathology and during treatment. We took advantage of its ubiquitous overexpression on the cancer cell surface and substantial underglycosylation, which reveals specific epitopes previously masked by oligosaccharides, making it possible to design probes with discriminating capacity between normal and breast tumor cells[20].

To detect uMUC-1-expressing tumors using noninvasive imaging, we have previously designed and synthesized a contrast agent (MN-EPPT) that consists of iron oxide nanoparticles (MN, detectable by magnetic resonance imaging, MRI), labeled with Cy5.5 dye for near-infrared optical imaging (NIRF) and conjugated to peptides (EPPT), specific for uMUC-1[21]. We have demonstrated the potential of MN-EPPT for the tracking of change in tumor size following chemotherapy in human xenograft models of pancreatic[22] and breast cancer[23]. We have also developed a method for the quantitative assessment of uMUC-1 expression based on the tumor-specific accumulation of MN-EPPT in breast tumors using noninvasive MRI[23].

Equipped with the ability to monitor changes in tumor size and in uMUC-1 expression noninvasively, in this study we investigated the stage-wise progression of breast cancer from pre-malignancy to malignancy in a well-defined transgenic mouse model of breast cancer (MMT)[24]. MMT mice express polyoma virus middle T (PyMT) and human MUC-1 double transgenes and develop spontaneous mammary carcinoma. In these mice, tumorigenesis

follows a progressive course characterized by pre-malignant (4–9 weeks), localized (10–16 weeks), and metastatic (after 16 weeks) stages similar to human breast cancer making them an ideal model for our research[24].

Using noninvasive imaging, we established that the uMUC-1 antigen is already altered in the premalignant stage and that its increasing alteration can be monitored over the course of the pathology. Furthermore, using our imaging approach we demonstrated downregulation of the uMUC-1 antigen following treatment with doxorubicin. We believe that the ability to monitor uMUC-1 noninvasively during the course of the disease and for the duration of therapy could serve as a valuable tool in choosing treatment options and in devising individualized therapy.

Materials and Methods

Probe synthesis and characterization

The uMUC-1–targeted MN-EPPT probe was synthesized and characterized as described in[21]. Peptide sequences were as follows: EPPT, C-AHA-A-R-E-P-P-T-R-T-F-A-Y-W-G-K (FITC). Synthesis resulted in a triple-labeled nanoparticle, consisting of FITC on EPPT peptide (for fluorescence microscopy), superparamagnetic iron oxide (MN, a magnetic reporter for MRI), and Cy5.5 dye (Amersham Biosciences) attached to the MN (for NIRF optical imaging). Iron concentration and peptide/FITC and Cy5.5 payloads were determined as described previously[21]. The resultant probe had an average iron concentration of 7.3 +/ 0.16 mg/mL (stock solution), 2.1 Cy5.5 molecules per nanoparticle, and 4.43 peptides per nanoparticle.

Transgenic breast cancer mouse model

C57BL/6 MUC1-Tg and MMT mice were kindly provided by Dr. S. Gendler (Mayo Clinic, Scottsdale, AZ). All mice were maintained in microisolator cages under specific pathogen-free environment at the Massachusetts General Hospital and treated in accordance with the guidelines of the Institutional Animal Care and Use Committee of the Massachusetts General Hospital. The transgenic mouse strains included: 1) MUC1 transgenic mice (MUC1) expressing MUC-1 in a tissue-specific fashion similar to that in humans without developing any cancer (n=5); 2) MMT mice (8-wk old, n=5 and 15-wk old, n=5) expressing PyMT and human MUC-1 double transgenes and developing spontaneous mammary carcinoma similar to that in humans[24].

All mice are congenic on the C57/BL6 background. The mice were selected for expression of the PyMT oncogene and/or MUC1 by PCR. Only female mice either positive for MT (MT mice) or MT/MUC1 double transgenes (MMT mice) were used for the experiments. MMT mice can exhibit hyperplasia by 4–9 weeks of age. Tumors appear between 10 and 16 weeks. Fully differentiated adenocarcinoma with lung and bone marrow metastasis arises by 17–24 weeks of age[24]. Only MMT mice that developed tumors were included in the study.

In vivo MR imaging

MR imaging was performed in both MMT and MUC1 mice at 8 weeks of age when there were no detectable tumors in either group and 15-wks of age, when MMT mice have a palpable tumor. For MRI, mice were injected intravenously with the uMUC-1-targeted MN-EPPT probe (10 mg Fe/kg). MR imaging was performed before and 24 hr after injections, using a 9.4T Bruker horizontal bore scanner (Billerica, MA) equipped with ParaVision 3.0 software. The imaging protocol consisted of coronal and transverse T2-weighted spin echo (SE) pulse sequences.

To produce T2 maps for quantitative analysis of probe accumulation, the following imaging parameters were used: SE TR/ TE = 3,000/[8, 16, 24, 32, 40, 48, 56, 64]; FOV, 40 × 40 mm; matrix size, 128 × 128; slice thickness, 0.5 mm and in-plane resolution, 312 × 312 μm. Image reconstruction and analysis were performed using Marevisi 3.5 software (Institute for Biodiagnostics, National Research Council, Canada). T2 maps were reconstructed, according to established protocol, by fitting the T2 values for each of the 8 echo times (TE) to a standard exponential decay curve.

Visual inspection of T2-weighted images was performed and mammary fat pads/tumors were analyzed by placing an ROI manually over the fat pad/tumor. The fat pad could be identified unambiguously on the T2-weighted MR images because its long native T2 relaxation times (pre-contrast) distinguish it from surrounding skin and muscle. In addition, surrounding anatomical structures were used to define the position of the fat pad and to retain consistency between imaging sessions. Quantitative evaluation of tumor size by MRI was based on multislice T2-weighted images and involved counting the number of pixels in each slice of the tumor ROI, adding up the total number of tumor ROI pixels across slices and multiplying by voxel volume. Relative MN-EPPT accumulation in the tumors was estimated based on the formula: T2 before injection minus T2 after injection (delta-T2, ms), as previously described[23].

In vivo optical imaging

In vivo NIRF optical imaging was done immediately after each MRI session. Animals were placed prone into a whole-body animal imaging system (IVIS Spectrum, Caliper/Perkin Elmer Company), equipped with 10 narrow band excitation filters (30-nm bandwidth) and 18 narrow band emission filters (20-nm bandwidth) that assist in significantly reducing autofluorescence by the spectral scanning of filters and the use of spectral unmixing algorithms. Imaging was performed using a 675-nm excitation and a 720-nm emission filter. The fluorescence imaging settings (exposure time, 0.5 seconds; F-stop, 2; binning, medium) were kept constant for comparative analysis. Grayscale white-light photographs and epifluorescent images were acquired and superimposed. The images were reconstructed using the Living Image software version 3.1 (Caliper/Perkin Elmer Company). A region of interest (ROI) was manually selected over relevant regions of signal intensity. The region of interest was defined based on anatomical photographs taken prior to acquisition of the NIRF images. The area of the ROI was kept constant, and the intensity was recorded as maximum photon counts within an ROI.

Doxorubicin (Dox) treatment

To establish a clinically relevant treatment model, we used the standard chemotherapeutic agent doxorubicin. The treatment protocol involved i.v. injections of 7 mg/kg of doxorubicin in saline solution once weekly for 2 consecutive weeks (16 and 17 weeks of age, 1 week after tumor appearance, n=3). PBS injected animals served as nontreated controls (n=3). As previously described, to evaluate tumor response to chemotherapy, in vivo imaging was done 24h before the beginning of treatment and 24h after the completion of treatment[23]

Histologic examination of tumors (Ex Vivo)

To detect the accumulation of MN-EPPT in tumor tissue, tumors were embedded in Tissue-Tek optimum cutting temperature compound (Sakura Fineteck) and snap frozen in liquid nitrogen. Tumors were then cut into 7-μm frozen sections, fixed in 2% paraformaldehyde, incubated with MN-EPPT (50μg/ml Fe overnight), washed, counterstained with Vectashield mounting medium with 4’,6-diamidino-2-phenylindole (DAPI; Vector Laboratories), and analyzed by fluorescence microscopy. Microscopy was done using a Nikon Eclipse 50i fluorescence microscope equipped with an appropriate filter set (Chroma Technology

Corporation). Images were acquired using a charge-coupled device camera with near-IR sensitivity (SPOT 7.4 Slider RTKE, Diagnostic Instruments) and analyzed using SPOT 4.0 advanced version software (Diagnostic Instruments).

Western Blotting

Frozen MMT tumor specimens were thawed and homogenized in tissue protein extraction lysis buffer (Tissue-PE LB from G-Biosciences, St Louis, MO) containing 1mM PMSF and proteinase inhibitor cocktails (Sigma). Protein content was determined with the Bio-Rad protein assay kit (Bio-Rad, Hercules, CA). Twenty micrograms of total protein from each sample was applied onto an SDS-polyacrylamide gel (4–20%) under reducing conditions. Rainbow marker (Amersham Life Science, Arlington Heights, IL) was used as a high molecular weight standard. Resolved proteins were transferred electrophoretically to nitrocellulose membranes and pre-blocked with 5% nonfat dry milk in Tris-buffered saline (TBS) for 1h at room temperature. After blocking the membrane was incubated overnight at 4°C in 1% milk/TBS containing monoclonal anti-human MUC1 antibody (1μg/ml; C595 (NCRC48), Abcam, Cambridge, MA). The membrane was then washed 3 times with 0.05% Tween TBS (TBST) and incubated with horseradish peroxidase-conjugated goat anti-mouse IgG (Invitrogen, Camarillo, CA) for 60 minutes at room temperature, followed by washing 3 times with TBST and one time with TBS. Membranes were developed using ECL Plus Western Blotting detection reagents kit (GE Healthcare, Piscataway, NJ) according to the manufacturer's specifications.

Immunofluorescence staining of poly (ADP-ribose) polymerase (PARP) and uMUC-1

Immunostaining for PARP was performed on 7-micron thick tumor tissue sections fixed in 2% paraformaldehyde for 10 min. The tissues were incubated with anti-cleaved PARP antibody (Cell signaling, Danvers, MA) followed by Texas Red-conjugated goat anti-rabbit immunoglobulin (Santa Cruz Biotechnology). Nuclear counterstaining with DAPI was performed after removal of excess secondary antibody. Immunostaining was examined under a fluorescence microscope as described above. To detect the level of uMUC-1 expression, tumor tissue sections were incubated with anti-MUC1 mouse antibody (C595 (NCRC48) Abcam, Cambridge, MA) followed by incubation with FITC-goat anti-mouse antibody (Santa Cruz Biotechnology). After DAPI nuclear staining, slides were analyzed by fluorescence microscopy.

Immunohistochemistry of human breast cancer tissue microarray (TMA)

Differential binding of MN-EPPT to human tissues with breast adenocarcinomas (CHTN, NIH) *versus* healthy control tissues was visualized by fluorescence microscopy. TMA slides representative of non-cancer, adjacent normal, ductal carcinoma in situ (DCIS), invasive ductal carcinoma (IDC) and lymph node metastases were deparaffinized in xylene for 10 min (2 × 5min) and then gradually rehydrated in a series of alcohol baths (100, 95, and 75%) and in distilled water. To improve antigen retrieval the samples were treated with 10mM sodium citrate buffer (pH 6.0) at 100°C for 10 min. The samples were washed with phosphate buffered saline (PBS; pH 7.2) and incubated in 3% blocking serum (goat or horse) for 1h to prevent non-specific antigen binding. The samples were then incubated with MN-EPPT (50μg/ml Fe) overnight at 4°C. After washing in PBS, slides were counterstained with Vectashield mounting medium with DAPI. The fluorescence stained slides were initially identified under a bright-field microscope and then subjected to correlative dual-channel fluorescence microscopy in the green (for FITC detection in EPPT peptides), as described above. For uMUC-1 visualization, the samples were incubated with a mouse monoclonal antibody specific for human MUC1 (clone: VU4H5) (Zymed Lab; Invitrogen) diluted 1:100 in PBS containing 1.5% horse serum Slides were incubated overnight at 4°C. Following, the slides were washed three times (5 min each) in PBS before incubation with

biotinylated horse-anti mouse immunoglobulins (DAKO) for 45 min at room temperature. The sections were washed three times for 5 min in PBS before 45 min incubation in an avidin–biotin–peroxidase complex (ABC) reagent (Vectastain ABC Elite kit; Vector Laboratories, Burlingame, CA). uMUC1 expression was visualized applying liquid DAB (ImmPACT DAB; DAKO) for up to 2min. Slides were rinsed in distilled water to stop the brown-colored reaction. The stained slides were immersed for 1 min. in aqueous hematoxylin (Sigma) to counterstain cell nuclei. Finally, the slides were washed in deionized water and dehydrated in a series of graded ethanol (75, 95 and 100%) baths before being rinsed in xylene (2×5min) and mounted in clear slides using permount (Sigma). Finally the slides were examined under light microscopy.

Statistical analysis

All data were represented as mean ± SD. Statistical analysis was done using two-tailed Student's t test and linear regression where indicated. $P<0.05$ was considered statistically significant.

Results

Noninvasive imaging of the transition to malignancy in the MMT mouse model

To distinguish between non-cancer and premalignant lesions and to detect the transition from pre-malignancy to malignancy noninvasively, we performed MRI and near-infrared optical imaging of non-tumor bearing (MUC1 transgenic), pre-malignant (8-wk old MMT) and tumor-bearing (15-wk old MMT) mice using MN-EPPT as a contrast agent. Since MUC1 transgenic mice do not develop tumors and therefore do not accumulate MN-EPPT, the T2 relaxation times of their mammary fat pads were long (Fig. 1A). These values were defined as "baseline". In contrast, the T2s of the mammary fat pads of 8-wk old MMT mice (pre-malignant) were significantly shorter ($p < 0.05$, Fig. 1A and B), indicating that MN-EPPT can be used to differentiate between non-cancer and pre-malignant lesions. With lesion progression to overt malignancy (15 wk old MMT mice), there was a further shortening of the T2 relaxation times of mammary tissue that was significant ($p < 0.05$, Fig. 1A and B).

These findings were also validated by in vivo NIRF optical imaging carried out immediately after each MRI session. Based on this analysis, it was evident that the fluorescence intensity of the mammary fat pads was lowest in the 8-wk old MUC1 transgenic mice, higher in 8-wk old MMT mice, and the highest in 15-wk old MMT mice, reflecting a progressively higher accumulation of MN-EPPT ($p < 0.05$, Fig. 2A and B). The tumor accumulation of the probe was also confirmed histologically (Fig. 2C).

To establish if, indeed, the age-differential accumulation of MN-EPPT reflected a histological transition from non-cancer to pre-malignancy, and malignancy, we analyzed tissues from the studied mice by histopathology, which represents the gold-standard method for this purpose. This analysis confirmed the characterization of the tissues as non-cancer (8-wk old MUC1), pre-malignant (8-wk old MMT) and malignant (15-wk old MMT mice; Suppl. Fig. 1A). Changes in the histological characteristics of these lesions correlated with the expression of uMUC-1 as shown by staining for this antigen (Suppl. Fig. 1B). Whereas in MUC1 mice, there was weak staining for uMUC-1 associated with the glandular epithelium, in the hyperplastic tissue of 8-wk old MMT mice there was a significant expression of the antigen over the disordered apical and basolateral glandular epithelium. In tumor tissue from 15-wk old MMT mice, the glandular architecture was not distinguishable any longer and expression of uMUC-1 was ubiquitous throughout the tissue (Suppl. Fig. 1B).

Collectively these findings indicated that our approach could 1) distinguish non-cancer from pre-malignancy and 2) monitor the transition from pre-malignancy to malignancy.

Noninvasive imaging of uMUC-1 downregulation in response to chemotherapy

uMUC-1 downregulation is a critical factor indicating tumor response to chemotherapy. To investigate whether uMUC-1 downregulation can be monitored noninvasively, we treated MMT mice with doxorubicin or PBS as a control. After completion of the treatment, we performed MRI before and after MN-EPPT injection. Probe accumulation was verified by the shortening of the tumor T2 relaxation times (Fig. 3A). Analysis of tumor delta-T2 values (T2 pre- T2 post-contrast) revealed significantly shorter delta-T2 values in doxorubicin-treated mice vs. PBS treated controls (14±2.8msec vs. 31.8±4.5msec respectively, Fig. 3B), indicating a reduced relative probe uptake by the tumor and suggesting reduced uMUC-1 expression in these animals. Indeed, the observations from imaging correlated with a lower level of uMUC-1 in doxorubicin-treated mice as confirmed by Western blotting (Fig. 3C). Importantly, treatment with doxorubicin led to tumor regression, as measured by both MRI (Fig. 4A) and optical imaging (not shown), reflective of increased levels of apoptosis in the tissue (Fig. 4B).

Clinical evaluation of MN-EPPT accumulation in human breast tissue

Since iron oxide nanoparticles have already been used in clinical trials for imaging cancer patients[25] we anticipate that our approach has an immediate clinical relevance. As a first step in this direction we evaluated human breast tissue microarrays representative of different stages of breast cancer (CHTN, NIH) for binding to the MN-EPPT probe. After incubation we observed differential probe accumulation in tumors at various stages of carcinogenesis (Fig. 5, top). Whereas control tissue (normal, no cancer history) showed limited binding of MN-EPPT, accumulation of the probe increased noticeably in adjacent normal (cancer history) and malignant tissue. This uptake correlated with uMUC-1 protein expression (Fig. 5, bottom). These results raised the intriguing possibility that uMUC-1 is altered in adjacent normal tissue from patients with cancer history relative to non-cancer patients, indicating that it is a very early marker of transformation. This possibility is now being explored in our laboratory in a separate study.

Discussion

A major focus of the breast cancer research and clinical communities is on defining the functional, cellular, and molecular characteristics of breast lesions to augment and refine the classification of these lesions for determinations of risk of tumor progression and therapeutic response. Furthermore, the ability to identify early molecular changes in breast tissue towards malignancy and to follow these changes during the course of therapy noninvasively would tremendously aid clinical researches. Towards that goal, we investigated the possibility to monitor changes in the underglycosylated mucin-1 tumor antigen, which represents a prominent hallmark of breast cancer progression.

High-resolution imaging methods in combination with tumor antigen-specific contrast agents are necessary to follow tumor progression on a molecular level. In our study we utilized a dual-modality imaging approach (MRI/NIRF) to monitor the relative availability of the uMUC-1 tumor antigen. uMUC-1 provides a unique advantage in this case because out of the major breast-cancer associated antigens, e.g. ER and Her2/neu, it demonstrates changes directly linked to breast cancer progression from the earliest in situ lesion to a metastatic disease, as well as to therapeutic outcome.

The dual modality approach combines the high-spatial resolution, tomographic capability, and unlimited tissue penetration of MRI with the high sensitivity, and low cost of in vivo optical imaging, as a validation tool. The clinical relevance of MRI, in particular, is well established. By using an iron oxide contrast agent, which provides a relatively high sensitivity of detection[26], and a high-field imaging system, we are exploring the current limits of MRI as a molecular imaging modality. Specifically, by monitoring the expression of a molecular biomarker, we obtain not only qualitative information about tumor size, but also quantitative information about the relative bioavailability of that biomarker within a lesion. This quantitative measurement can serve as an indicator of the stage of progression of that lesion, as well as the likelihood that it will develop into full-blown metastatic disease or that it would respond to therapeutic intervention.

In the context of other MR-suitable contrast agents, the present probes represent a clear advantage. Whereas paramagnetic contrast agents are only effective for detection at high concentrations (>0.1 mM)[27], superparamagnetic agents, such as MN-EPPT, have constant R2 relaxivity values at field strengths over 0.5T[28] and are associated with a high nanomolar sensitivity of detection. In cell labeling studies, in vivo detection of a single cell labeled with superparamagnetic iron oxide nanoparticles has been achieved[29]. In addition, superparamagnetic iron oxides have a proven safety record and are used extensively in a clinical setting. Finally, these agents represent a versatile platform which, through modifications in the size and surface coating of the nanoparticles, can be used to design molecularly targeted probes for the detection and characterization of specific cell subpopulations and/or biochemical processes[21], long circulating contrast agents for mapping of the vasculature[30], multifunctional probes for image-guided therapeutics[31, 32], or for cell tracking[33].

With specific regard to the present study, we have previously employed both types of contrast agent for the detection of primary tumors in small animals. In comparison to gadolinium (Gd)-DTPA (a paramagnetic T1 contrast agent)[34], the iron oxide-based MN-EPPT effectively resulted in lowering the detection threshold for lesions to 3mm[3 22]

Overall, our approach could not only help identify the earliest signs of molecular dysregulation representative of breast cancer but also unravel some of the complex molecular pathways leading up to the development of the pathology. Also our studies establish the feasibility of a novel multi-parameter method for monitoring breast cancer response to chemotherapy, based on the expression of molecular markers implicated in disease progression from an in situ to an invasive and a metastatic phenotype. Finally, considering that related iron oxides are already in clinical use[25], the developed technology may ultimately become applicable in a clinical setting and as such has the potential of significantly advancing our ability to diagnose breast cancer at the earliest stages of the pathology, before any overt clinical symptoms have developed, as well as to better direct the development of molecularly-targeted individualized therapy protocols.

On a broader scale, our studies are important because they offer the possibility for predictive cancer diagnosis. Progress has already been made in that direction. An example includes screening for the BRCA mutation for the assessment of breast cancer risk[35]. With specific relevance to noninvasive imaging, a glimpse into the potential of this technology derives from the development of dynamic MRI techniques[36], magnetic resonance spectroscopy[37], and positron emission tomography[38]. Still, none of these technologies probe for specific molecular biomarkers expressed by cells in proportion to their potential for malignancy. It is this highly specific molecular imaging approach that has the potential of capturing the premalignant condition and permitting preventive rather than curative therapeutic intervention.

Supplementary Material

Refer to Web version on PubMed Central for supplementary material.

Acknowledgments

This study was supported in part by the NIH grant award 1RO1CA135650 to A.M and Z.M.

References

1. Xing P, Tjandra J, Stacker S, Teh J, Thompson C, McLaughlin P, McKenzie I. Monoclonal antibodies reactive with mucin expressed in breast cancer. Immunol Cell Biology. 1989; 67(Pt 3): 183–195.
2. Hayes D, Mesa-Tejada R, Papsidero L, Croghan G, Korzun A, Norton L, Wood W, Strauchen J, Grimes M, Weiss R, Ree H, Thor A, et al. Prediction of prognosis in primary breast cancer by detection of a high molecular weight mucin-like antigen using monoclonal antibodies DF3, F36/22, and CU18: a Cancer and Leukemia Group B study. J Clin Oncol. 1991; 9:1113–1123. [PubMed: 2045853]
3. Perey L, Hayes D, Maimonis P, Abe M, O'Hara C, Kufe D. Tumor-specific reactivity of a monoclonal antibody prepared against a recombinant peptide derived from the D3 human breast carcinoma-associated antigen. Cancer Res. 1992; 52:2563–2568. [PubMed: 1373671]
4. Nacht M, Ferguson A, Zhang W, Petroziello J, Cook B, Hong Gao Y, Maguire S, Riley D, Coppola G, Landes G, Madden S, Sukumar S. Combining serial analysis of gene expression and array technologies to identify genes differentially expressed in breast cancer. Cancer Res. 1999; 59:5464–5470. [PubMed: 10554019]
5. Dede DS, Arslan C, Altundag K. Serum levels of CEA and CA 15-3 in triple-negative breast cancer at the time of diagnosis. Med Oncol. 2010; 27:1429. [PubMed: 19774500]
6. Park S, Ahn HK, Park LC, Hwang DW, Ji JH, Maeng CH, Cho SH, Lee JY, Park KT, Ahn JS, Park YH, Im YH. Implications of different CA 15-3 levels according to breast cancer subtype at initial diagnosis of recurrent or metastatic breast cancer. Oncology. 2012; 82:180–187. [PubMed: 22433564]
7. McGuckin MA, Walsh MD, Hohn BG, Ward BG, Wright RG. Prognostic significance of MUC1 epithelial mucin expression in breast cancer. Hum Pathol. 1995; 26:432–439. [PubMed: 7705823]
8. Croce MV, Colussi AG, Price MR, Segal-Eiras A. Expression of tumour associated antigens in normal, benign and malignant human mammary epithelial tissue: a comparative immunohistochemical study. Anticancer Res. 1997; 17:4287–4292. [PubMed: 9494522]
9. Yonezawa S, Sato E. Expression of mucin antigens in human cancers and its relationship with malignancy potential. Pathol Int. 1997; 47:813–830. [PubMed: 9503463]
10. Cao Y, Blohm D, Ghadimi BM, Stosiek P, Xing PX, Karsten U. Mucins (MUC1 and MUC3) of gastrointestinal and breast epithelia reveal different and heterogeneous tumor-associated aberrations in glycosylation. J Histochem Cytochem. 1997; 45:1547–1557. [PubMed: 9358856]
11. Barratt-Boyes S. Making the most of mucin: a novel target for tumor immunotherapy. Cancer Immunol Immunother. 1996; 43:142–151. [PubMed: 9001567]
12. Schroeder JA, Masri AA, Adriance MC, Tessier JC, Kotlarczyk KL, Thompson MC, Gendler SJ. MUC1 overexpression results in mammary gland tumorigenesis and prolonged alveolar differentiation. Oncogene. 2004; 23:5739–5747. [PubMed: 15221004]
13. Mommers E, Leonhart A, Silvia, Von Mensdorff-Pouilly S, Schol D, Hilgers J, Meijer C, Baak J, Van Diest P. Abberant expression of MUC1 mucin in ductal hyperplasia and ductal carcinoma in situ of teh breast. Int J Cancer. 1999; 84:466–469. [PubMed: 10502721]
14. de Roos MA, van der Vegt B, Peterse JL, Patriarca C, de Vries J, de Bock GH, Wesseling J. The expression pattern of MUC1 (EMA) is related to tumour characteristics and clinical outcome in 'pure' ductal carcinoma in situ of the breast. Histopathology. 2007; 51:227–238. [PubMed: 17650217]

15. Al-azawi D, Kelly G, Myers E, McDermott EW, Hill AD, Duffy MJ, Higgins NO. CA 15-3 is predictive of response and disease recurrence following treatment in locally advanced breast cancer. BMC cancer. 2006; 6:220. [PubMed: 16953875]
16. Hanson JM, BroweIl DA, Cunliffe WJ, Varma J, Allen A, Hemming D, Shenton BK, Young JR, Higgs MJ, Brotherick I, Pearson JP. MUC1 expression in primary breast cancer: the effect of tamoxifen treatment. Breast Cancer Res Treat. 2001; 67:215–222. [PubMed: 11561767]
17. Yuan Z, Wong S, Borrelli A, Chung MA. Down-regulation of MUC1 in cancer cells inhibits cell migration by promoting E-cadherin/catenin complex formation. Biochem Biophys Res Commun. 2007; 362:740–746. [PubMed: 17764657]
18. Shi FF, Gunn GR, Snyder LA, Goletz TJ. Intradermal vaccination of MUC1 transgenic mice with MUC1/IL-18 plasmid DNA suppresses experimental pulmonary metastases. Vaccine. 2007; 25:3338–3346. [PubMed: 17292519]
19. Scholl S, Squiban P, Bizouarne N, Baudin M, Acres B, Von Mensdorff-Pouilly S, Shearer M, Beuzeboc P, Van Belle S, Uzielly B, Pouillart P, Taylor-Papadimitriou J, et al. Metastatic breast tumour regression following treatment by a gene-modified vaccinia virus expressing MUC1 and IL-2. J Biomed Biotechnol. 2003; 2003:194–201. [PubMed: 12975534]
20. Spicer A, Rowse G, Lidner T, Gendler S. Delayed mammary tumor progression in Muc-1 null mice. J Biol Chem. 1995; 270:30093–30101. [PubMed: 8530414]
21. Moore A, Medarova Z, Potthast A, Dai G. In vivo targeting of underglycosylated MUC-1 tumor antigen using a multimodal imaging probe. Cancer Res. 2004; 64:1821–1827. [PubMed: 14996745]
22. Medarova Z, Pham W, Kim Y, Dai G, Moore A. In vivo imaging of tumor response to therapy using a dual-modality imaging strategy. Int J Cancer. 2006; 118:2796–2802. [PubMed: 16385568]
23. Medarova Z, Rashkovetsky L, Pantazopoulos P, Moore A. Multiparametric monitoring of tumor response to chemotherapy by noninvasive imaging. Cancer Res. 2009; 69:1182–1189. [PubMed: 19141648]
24. Chen D, Xia J, Tanaka Y, Chen H, Koido S, Wernet O, Mukherjee P, Gendler SJ, Kufe D, Gong J. Immunotherapy of spontaneous mammary carcinoma with fusions of dendritic cells and mucin 1-positive carcinoma cells. Immunology. 2003; 109:300–307. [PubMed: 12757626]
25. Harisinghani M, Barentsz J, Hahn P, Deserno W, Tabatabaei S, van de Kaa C, de la Rosette J, Weissleder R. Noninvasive detection of clinically occult lymph-node metastases in prostate cancer. New Engl J Med. 2003; 348:2491–2499. [PubMed: 12815134]
26. Heyn C, Bowen CV, Rutt BK, Foster PJ. Detection threshold of single SPIO-labeled cells with FIESTA. Magn Reson Med. 2005; 53:312–320. [PubMed: 15678551]
27. Caravan P. Strategies for increasing the sensitivity of gadolinium based MRI contrast agents. Chem Soc Rev. 2006; 35:512–523. [PubMed: 16729145]
28. Sosnovik DE, Nahrendorf M, Weissleder R. Magnetic nanoparticles for MR imaging: agents, techniques and cardiovascular applications. Basic Res Cardiol. 2008; 103:122–130. [PubMed: 18324368]
29. Heyn C, Ronald JA, Mackenzie LT, MacDonald IC, Chambers AF, Rutt BK, Foster PJ. In vivo magnetic resonance imaging of single cells in mouse brain with optical validation. Magn Reson Med. 2006; 55:23–29. [PubMed: 16342157]
30. Wagner S, Schnorr J, Pilgrimm H, Hamm B, Taupitz M. Monomer-coated very small superparamagnetic iron oxide particles as contrast medium for magnetic resonance imaging: preclinical in vivo characterization. Invest Radiol. 2002; 37:167–177. [PubMed: 11923639]
31. Medarova Z, Kumar M, Ng S, Yang J, Barteneva N, Evgenov N, Petkova V, Moore A. Multifunctional magnetic nanocarriers for image-tagged siRNA delivery to intact pancreatic islets. Transplantation. 2008; 86:1170–1177. [PubMed: 19005396]
32. Medarova Z, Pham W, Farrar C, Petkova V, Moore A. In vivo imaging of siRNA delivery and silencing in tumors. Nat Med. 2007; 13:372–377. [PubMed: 17322898]
33. Arbab AS, Frank JA. Cellular MRI and its role in stem cell therapy. Regen Med. 2008; 3:199–215. [PubMed: 18307404]

34. Grimm J, Potthast A, Wunder A, Moore A. Magnetic resonance imaging of the pancreas and pancreatic tumors in a mouse orthotopic model of human cancer. International journal of cancer. Int J Cancer. 2003; 106:806–811. [PubMed: 12866043]

35. Bayraktar S, Elsayegh N, Gutierrez Barrera AM, Lin H, Kuerer H, Tasbas T, Muse KI, Ready K, Litton J, Meric-Bernstam F, Hortobagyi GN, Albarracin CT, et al. Predictive factors for BRCA1/BRCA2 mutations in women with ductal carcinoma in situ. Cancer. 2012; 118:1515–1522. [PubMed: 22009639]

36. Shin HJ, Baek HM, Ahn JH, Baek S, Kim H, Cha JH, Kim HH. Prediction of pathologic response to neoadjuvant chemotherapy in patients with breast cancer using diffusion-weighted imaging and MRS. NMR Biomed. 2012

37. Youk JH, Son EJ, Chung J, Kim JA, Kim EK. Triple-negative invasive breast cancer on dynamic contrast-enhanced and diffusion-weighted MR imaging: comparison with other breast cancer subtypes. Eur Radiol. 2012; 22:1724–1734. [PubMed: 22527371]

38. Vinh-Hung V, Everaert H, Lamote J, Voordeckers M, van Parijs H, Vanhoeij M, Verfaillie G, Fontaine C, Vees H, Ratib O, Vlastos G, De Ridder M. Diagnostic and prognostic correlates of preoperative FDG PET for breast cancer. Eur J Nucl Med Mol Imaging. 2012

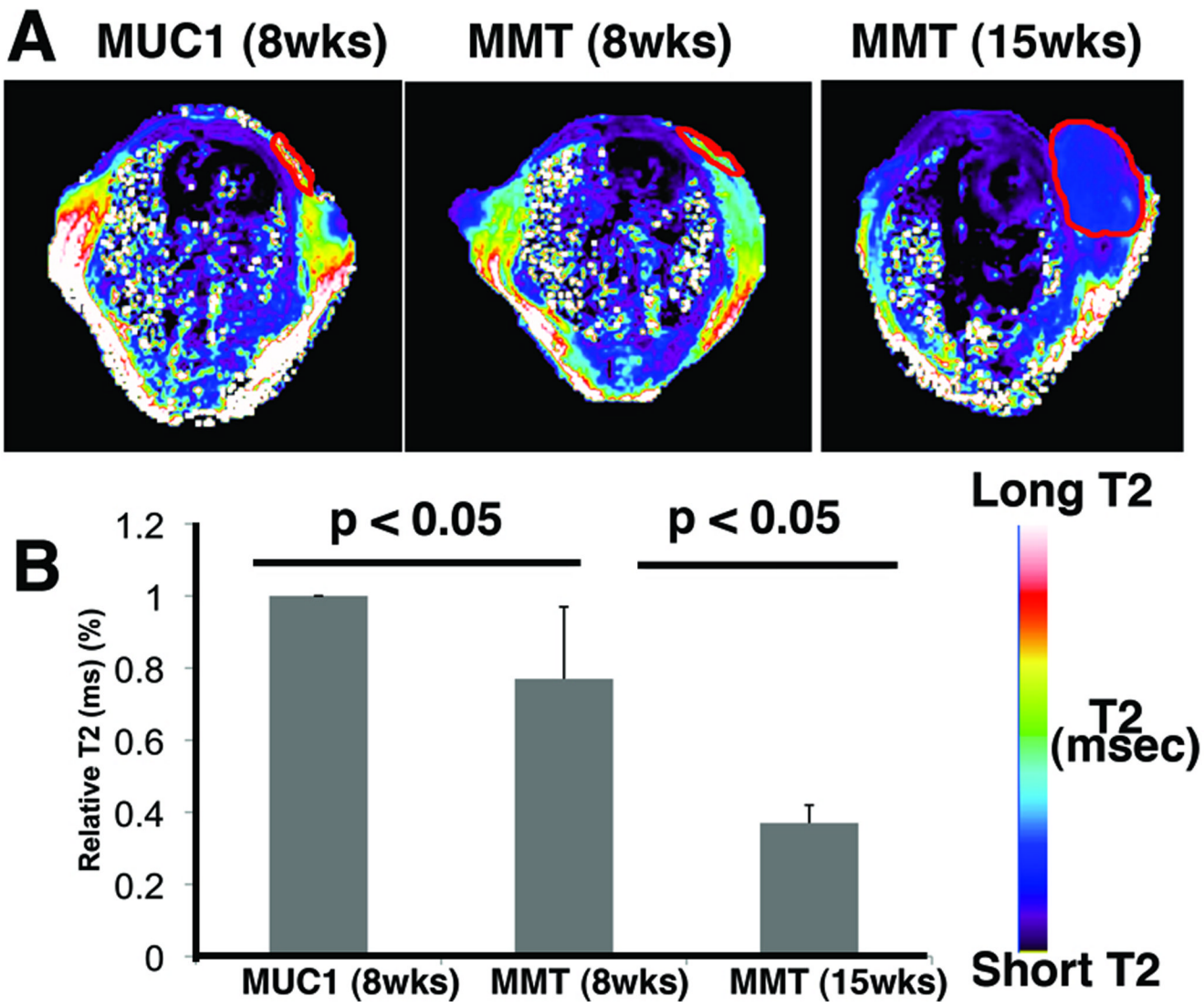

Fig. 1.

Magnetic resonance imaging of MN-EPPT accumulation in the mammary fat pads of transgenic MMT or MUC1 control mice. A. MRI. Representative color-coded T2 maps of mice (MUC1 and MMT) injected i.v. with MN-EPPT (10 mg/kg iron). There was a progressive loss of signal intensity (T2 shortening) between non-cancer (MUC1), premalignancy (8-wk MMT) and malignancy (15-wk MMT) in the mammary fat pads (outlined). B. Quantitative analysis of the T2 relaxation times, revealing that these differences are significant ($p<0.05$).

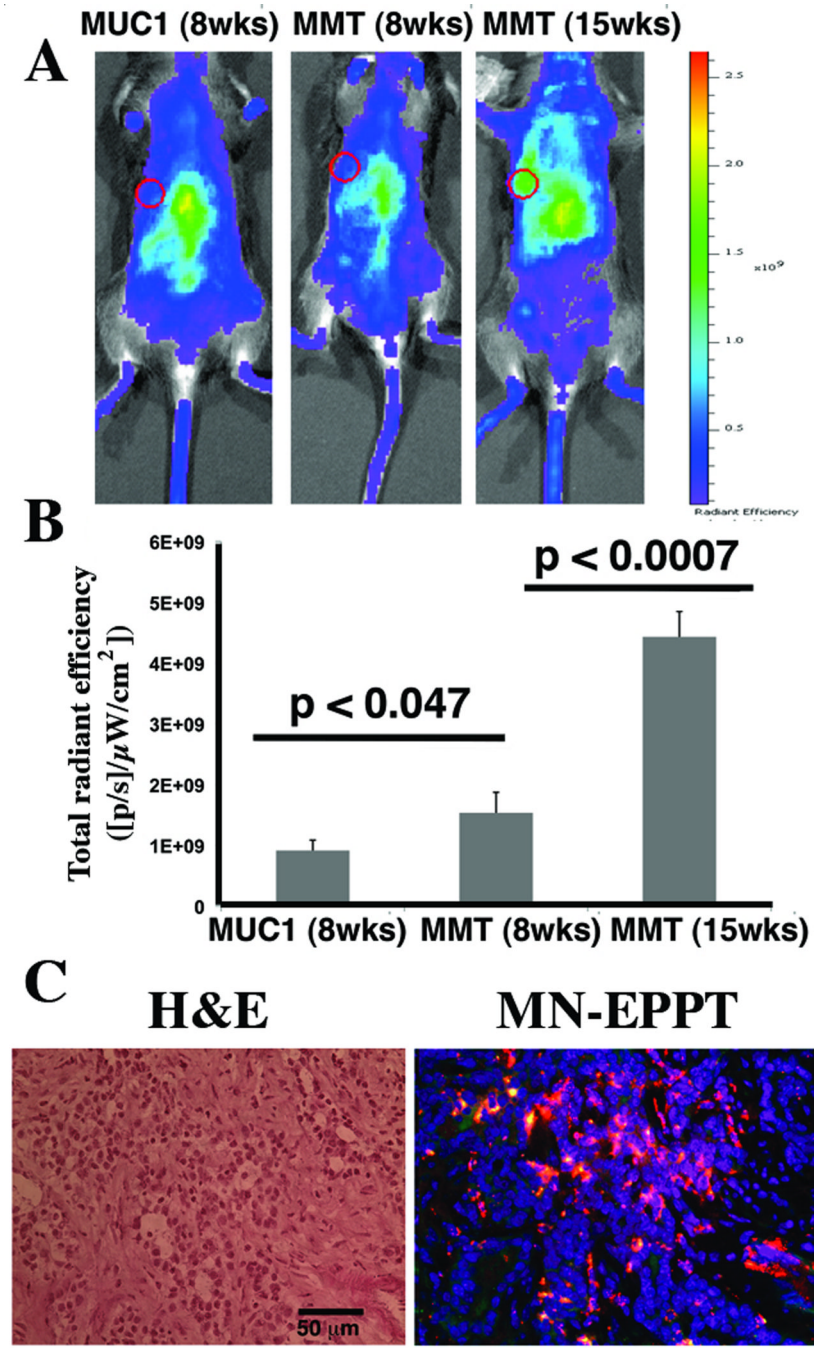

Fig. 2.

NIRF optical imaging of MN-EPPT accumulation in the mammary fat pads of transgenic MMT or MUC1 control mice. A. Representative color-coded fluorescent images of mice (MUC1 and MMT) injected i.v. with MN-EPPT. Individual fat pads are outlined. However, transformation occurs across multiple fat pads in a single animal. There was a progressive increase in signal intensity between non-cancer (MUC1), premalignancy (8-wk MMT) and malignancy (15-wk MMT). B. Quantitative analysis of radiant efficiency, revealing that these differences are significant ($p<0.05$). C. Fluorescence microscopy of MN-EPPT accumulation in tumor tissue, following intravenous injection of the probe (15-wk shown).

Images represent an overlay of green (FITC on EPPT), red (Cy5.5 on MN), and blue (DAPI, nuclei). Bar = 50μm.

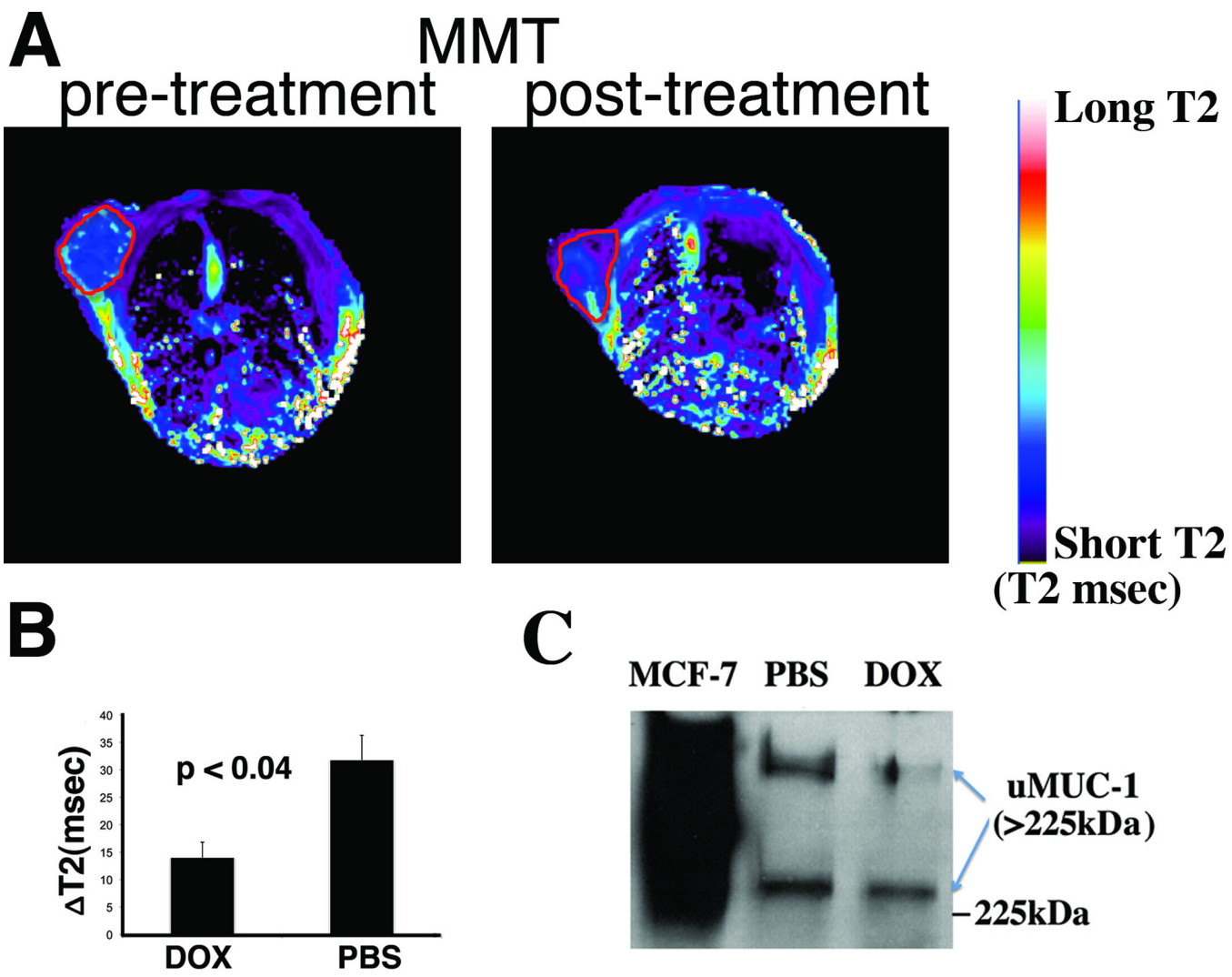

Fig. 3.

MRI of uMUC-1 expression in MMT tumors treated with doxorubicin. A. Representative T2-maps before and after injection treatment with doxorubicin. B. Delta-T2 values of DOX and PBS treated animals, revealing that in the presence of chemotherapy, delta-T2 values are significantly lower, indicating reduced MN-EPPT uptake. C. Western blotting confirming down-regulation of uMUC-1 in the presence of chemotherapy.

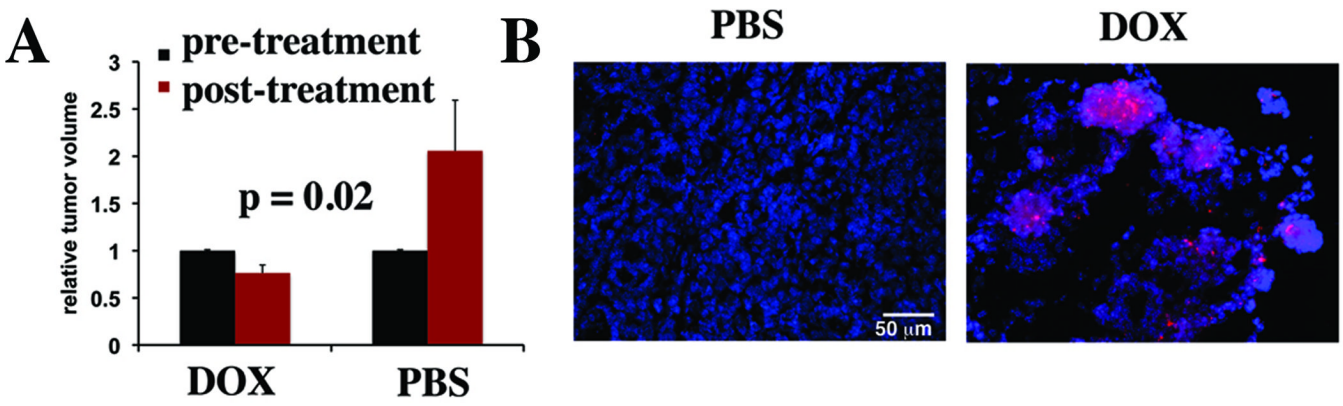

Fig. 4.

Noninvasive imaging of tumor volume during chemotherapy. A. MRI-derived quantitative analysis of tumor volume in DOX and PBS treated animals, revealing tumor regression in the DOX-treated animals and tumor growth in the PBS controls. B. Immunofluorescence to detect apoptosis (PARP cleavage) in tumors of MMT mice treated with chemotherapy.

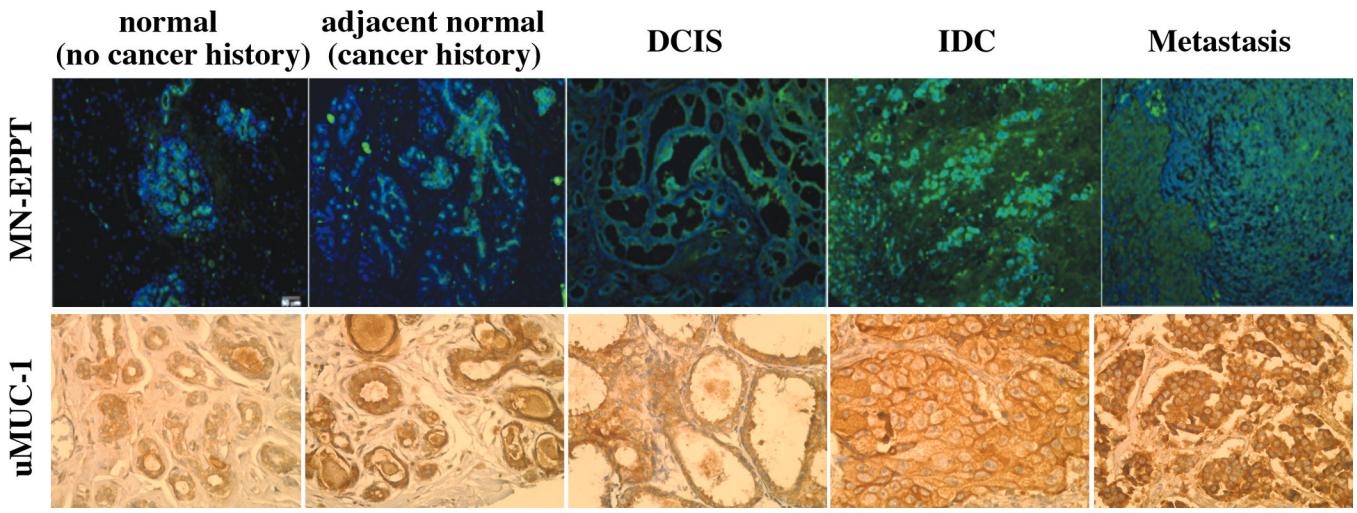

Fig. 5.

Top: Fluorescence microscopy of MN-EPPT accumulation in human tissue microarrays representative of breast cancer progression. Green, FITC on MN-EPPT. Bottom: Light microscopy of human breast tissue microarrays to detect uMUC-1. The microarrays were stained with antiserum that binds the underglycosylated MUC-1 (brown).